

Pearlite growth rate in Fe-C and Fe-Mn-C Steels

Seung-Woo Seo^a H. K. D. H. Bhadeshia^{a,b} Dong Woo Suh^a

^a*Graduate Institute of Ferrous Technology, POSTECH, Republic of Korea*

^b*Materials Science and Metallurgy, University of Cambridge, U.K.*

Abstract

The kinetic theory for the growth of pearlite in binary and ternary steels is implemented to ensure local equilibrium at the transformation front with austenite, while accounting for both boundary and volume diffusion of solutes. Good agreement is on the whole observed with published experimental data, although the reported growth rate at the lowest of temperatures is much smaller than predicted. To investigate this, experiments were conducted to replicate the published data. It is found that the cooperation between cementite and ferrite breaks down at these temperatures, and surface relief experiments are reported to verify that the resulting transformation product is not bainite.

Key words: pearlite, kinetics, non-cooperative growth, surface relief, binary and ternary alloys

1 Introduction

Pearlite contributes to the success of many commercial steels, for example those for rails, ropes for bridges and elevators, and tyre cords. In three dimensions, a colony of pearlite is an interpenetrating bi-crystal of cementite and ferrite [1], often approximated to consist of alternating lamellae of ferrite and cementite. The characteristic feature of pearlite is the fact that the ferrite (α) and cementite (θ) grow cooperatively, sharing a common transformation front with austenite (γ), where the excess carbon partitioned into the austenite as the ferrite grows, is absorbed by the adjacent cementite. The passage of this carbon occurs via the austenite at the transformation front, so the growth of the colony is modelled assuming that the rate is controlled by diffusion in the austenite ahead of the front [2–6]. Diffusion in the interface can be faster, and there are models for pearlite growth involving boundary diffusion control [7, 8]. There is of course, no reason why the solute is limited to either the

volume or boundary, and there are models that deal simultaneously with both diffusion fluxes [9–11]. It has been suggested that diffusion behind the α/γ interface, towards the cementite, may also play a role [12], but this would lead to the thickening of the cementite behind the transformation front, and the evidence for such an effect is lacking. Strain resulting from the volume change has been claimed to reach 1000 MPa in the elastic limit, and only relieved by the diffusion of carbon. This stress driven diffusion thus accelerates the pearlite reaction [13]. The model is unphysical because it neglects the diffusion of iron that is necessary in a reconstructive transformation [14]; this relieves transformation strains including the volume change. In [13], the transformation in pure iron would be dramatically suppressed because to the absence of carbon diffusion, and this is patently not the case.

Assuming therefore, that the general problem is best treated by accounting for both the boundary and volume diffusion fluxes, there remain difficulties in dealing with ternary or higher order steels, especially if local equilibrium is assumed at the interphase boundaries. The well-known complication is that the diffusivities of the substitutional and interstitial solutes are vastly different, so unlike the case for binary steels, it becomes necessary to discover conditions where the two or more solute fluxes can keep pace whilst maintaining equilibrium locally at the interface [14–18]. This difficulty is discussed in more detail later in the text, but from an experimental point of view, there is no doubt that substitutional solutes are partitioned between the phases at all temperatures where pearlite is observed [19–21]. Pandit and Bhadeshia [11] found it necessary to make approximations when dealing with ternary alloys. Those estimations do not strictly satisfy the simultaneous conditions of local equilibrium and flux balance at all the interfaces involved in the growth of pearlite. In this paper we attempt to resolve this difficulty, bearing in mind that the kinetic theory for pearlite is of interest in many current scenarios [22–27].

2 Methods

The diffusion-controlled growth of pearlite in a binary steel, including both the volume and boundary fluxes, is given by [10]:

$$v = \left(2D_V + \frac{12sD_B\delta}{S} \right) \frac{S}{S_\alpha S_\theta} \left(\frac{c_e^{\gamma\alpha} - c_e^{\gamma\theta}}{c^{\theta\gamma} - c^{\alpha\gamma}} \right) \left(1 - \frac{S_C}{S} \right) \quad (1)$$

where v is the growth rate, s is the arbitrary length which is normal to growth direction, D_V and D_B are volume and boundary diffusion coefficients in austenite respectively, S is the interlamellar spacing, S_C is the critical interlamellar spacing when the α/θ interfaces that are created during pearlite

growth consume all the available free energy so that the growth rate becomes zero. $c^{\gamma\theta}$ is the concentration in austenite that is in equilibrium with cementite, and other terms like this have similar meaning. These equilibrium compositions are here calculated using ThermoCalc with the TCFE6 database [28].

In equation 1, the values of interlamellar spacing S , the diffusion coefficients and boundary thickness $\delta = 2.5 \text{ \AA}$ can be obtained from the published literature [5, 29–31]. The diffusivity of carbon in austenite is concentration dependent, so a weighted average value is used instead [32]:

$$\bar{D}_V = \int_{c^{\gamma\theta}}^{c^{\gamma\alpha}} \frac{D\{\bar{c}, T\}}{c^{\gamma\alpha} - c^{\gamma\theta}} dc^{\gamma} \quad (2)$$

where \bar{c} is the mean carbon concentration in the steel.

The situation is more complex for Fe-C-X steels containing a substitutional solute (X) in addition to interstitial carbon. Local equilibrium requires the compositions at the interface to be maintained at levels that are consistent with a tie-line of the Fe-C-X phase diagram. At a constant temperature, this is in general not possible to achieve for the tie line passing through $\bar{c}_{\text{Mn}}, \bar{c}_{\text{c}}$ because the rate at which each solute is partitioned must then equal to that at which it is carried away from the interface by diffusion. It is necessary therefore that

$$\text{at } \alpha/\gamma \text{ interface: } \begin{cases} v(c_{\text{C}}^{\gamma\alpha} - c_{\text{C}}^{\alpha\gamma}) = -D_{\text{C}} \nabla c_{\text{C}} \\ v(c_{\text{Mn}}^{\gamma\alpha} - c_{\text{Mn}}^{\alpha\gamma}) = -D_{\text{Mn}} \nabla c_{\text{Mn}} \end{cases} \quad (3)$$

$$\text{at } \theta/\gamma \text{ interface: } \begin{cases} v(c_{\text{C}}^{\gamma\theta} - c_{\text{C}}^{\theta\gamma}) = -D_{\text{C}} \nabla c_{\text{C}} \\ v(c_{\text{Mn}}^{\gamma\theta} - c_{\text{Mn}}^{\theta\gamma}) = -D_{\text{Mn}} \nabla c_{\text{Mn}} \end{cases} \quad (4)$$

where the subscripts identify the solute. Given that $D_{\text{Mn}} \ll D_{\text{C}}$, it becomes impossible to simultaneously satisfy either equation 3 or 4 if the tie-line passing through $\bar{c}_{\text{Mn}}, \bar{c}_{\text{c}}$ is selected.

Pandit and Bhadeshia [11] argued that in the context of experimental data, local equilibrium could not be assumed for both the α/γ and θ/γ interfaces. They therefore proceeded to adopt the tie line connecting the θ/γ interface passes through $\bar{c}_{\text{Mn}}, \bar{c}_{\text{c}}$ (Fig. 1), neglected the role of carbon and calculated the growth rate on the basis of the diffusion of manganese through the interfaces rather than the volume ahead of the interface.

A different procedure avoiding the difficulties encountered in ref. [11], can be based on the following equations that are analogous with equation 1:

$$\begin{aligned}
 v_C &= \left(2D_V^C + \frac{12sD_B^C\delta}{S} \right) \frac{S}{S_\alpha S_\theta} \left(\frac{c_C^{\gamma\alpha} - c_C^{\gamma\theta}}{c_C^{\theta\gamma} - c_C^{\alpha\gamma}} \right) \left(1 - \frac{S_C}{S} \right) \\
 v_{Mn} &= \left(2D_V^{Mn} + \frac{12sD_B^{Mn}\delta}{S} \right) \frac{S}{S_\alpha S_\theta} \left(\frac{c_{Mn}^{\gamma\alpha} - c_{Mn}^{\gamma\theta}}{c_{Mn}^{\theta\gamma} - c_{Mn}^{\alpha\gamma}} \right) \left(1 - \frac{S_C}{S} \right)
 \end{aligned} \quad (5)$$

where the velocities v_C and v_{Mn} are calculated on the basis of the diffusion of only carbon or only manganese, respectively. Clearly, since there is only one transformation front, the equations must be solved such that $v_C = v_{Mn}$. Bearing in mind that the interlamellar spacing is also identical in these equations, a further condition arises that:

$$\frac{D_C}{D_{Mn}} = \frac{R_{Mn}}{R_C} \quad \text{with} \quad \begin{cases} D_i \equiv D_V^i + \frac{6sD_B^i\delta}{S} \\ R_i \equiv \frac{c_i^{\gamma\alpha} - c_i^{\gamma\theta}}{c_i^{\theta\gamma} - c_i^{\alpha\gamma}} \end{cases} \quad (6)$$

The R_i condition ensures that the weighted average of the ferrite and cementite yields the mean composition of the steel. With these two constraints and in addition the local equilibrium condition, it has been found possible to find unique interface compositions at the growth front by coupling the conditions and the velocity equations to thermodynamic calculations using Thermo-Calc with TCFE6 database; the application package was designed as follows:

- a trial θ/γ interface composition is set, selected from possible such tie-lines for the given transformation temperature.
- The α/γ interface composition tie-line is selected such that $\overline{c_{C,Mn}^{\alpha\gamma}}, \overline{c_{C,Mn}^{\theta\gamma}} \ni \overline{c_{C,Mn}^{\alpha\gamma}}$ (where $\overline{c_{C,Mn}^{\alpha\gamma}}, \overline{c_{C,Mn}^{\theta\gamma}}$ means the line connecting the compositions of ferrite and cementite, and $\overline{c_{C,Mn}}$ is average composition in the system).
- If equation 6 is not satisfied by these choices then the process is repeated until a solution is found.
- This solution provides the interface compositions to substitute into equation 5 to calculate the single velocity $v = v_C = v_{Mn}$ of the transformation interface.

3 Results and Discussion

3.1 Mixed diffusion controlled pearlite growth in Fe-C

There are several methods that can be used for measuring the growth rate of pearlite: particle size analysis method [30], the maximum nodule radius method [33] and the Cahn & Hagel method [34]. Neutron depolarisation [35] and three-dimensional X-ray microscopy [36] can also be used to measure

individual colony growth rates. The experimental data of Frye *et al.* [29] based on the maximum nodule radius method were used to obtain the boundary diffusion coefficient of carbon. This is because the method is based on the assumption that the largest module correctly represents the actual growth rate, whereas the other two methods rely on averaged values. The term $\frac{S_C}{S}$ was calculated by taking derivative of equation 1 with respect to the interlamellar spacing, S , and solving the resulting equation for S_C that satisfies:

$$\frac{dv}{dS} = 0 \quad (7)$$

Equations 1 and 7, when used with the experimental value of v , have two unknowns. They can therefore be solved iteratively to find the values of D_B and $\frac{S_C}{S}$.¹ As a result, the boundary diffusion coefficient for carbon is found to be

$$D_B^C = 1.84 \times 10^{-3} \exp\left(-\frac{124995 \text{ J mol}^{-1}}{RT}\right) \quad \text{m}^2 \text{ s}^{-1} \quad (8)$$

where R is the gas constant and T is the temperature, in Fig. 2. The boundary diffusion activation energy, $Q_B = 125 \text{ kJ mol}^{-1}$, is lower, as it should be, than the corresponding value for diffusion in the volume of the austenite, $Q_V = 135 \text{ kJ}$.

Fig. 3 shows calculations based on equation 1 and the experimental data of Brown and Ridley [30], and Frye *et al.* [29]. The carbon diffusion coefficient derived using Frye's data has been applied unmodified to the data from Brown and Ridley, and yet there is excellent closure between experiment and theory. Fig. 4 illustrates the ratio of volume to boundary diffusion fluxes and the dependence of S on the transformation temperature. As expected, the boundary flux dominates at low temperatures where diffusion within the austenite lattice is relatively sluggish. Fig. 4b is the set of all solutions which satisfying equation 7. When D_V is negligible relative to D_B , $\frac{S_C}{S}$ tends towards $\frac{2}{3}$ in the low temperature range.

3.2 Mixed diffusion-controlled growth for Fe-Mn-C

The diffusion coefficients of manganese in the boundary and austenite are from Fridberg *et al.* [37]:

$$D_B^{Mn} = 2.16 \times 10^{-4} \exp\left(-\frac{155000 \text{ J mol}^{-1}}{RT}\right) \quad \text{m}^2 \text{ s}^{-1} \quad (9)$$

¹ *Mathematica* source code freely available on www.msm.cam.ac.uk/map/mapmain.html

$$D_V^{Mn} = 1.34 \times 10^{-4} \exp\left(-\frac{286000 \text{ J mol}^{-1}}{RT}\right) \quad \text{m}^2 \text{ s}^{-1} \quad (10)$$

There will be some uncertainty in D_{Mn}^B because it is assumed to be identical to that for the grain boundary diffusion of iron [37]. Equation 1 for the ternary system was tested against experimental data on 1 wt% Mn and 1.8 wt% Mn eutectoid steels from the work of Razik and Ridley [31].

As shown in Fig. 5, the mixed diffusion controlled-growth model explains the pearlite growth rates within an order of magnitude. A careful examination of the tie-lines operating during growth showed that at low temperatures, there is very little partitioning of manganese between the phases and partitioning becomes prominent for transformation at temperatures near the eutectoid. The extent of partitioning is predicted well using our mixed diffusion model, when compared against the microanalytical data of Hutchinson *et al.* [21] for Fe-3.50Mn-2.46C at.% steel at 898 K [21], Fig. 6. It is likely that during the 10 h treatment, soft impingement occurs and that might explain the discrepancy observed for that transformation time. The measured growth rate was $1.08 \times 10^{-8} \text{ m s}^{-1}$, which compares well with our calculated value of $9.46 \times 10^{-9} \text{ m s}^{-1}$.

Table 1

Calculated Mn concentrations (at.%); the mean value for the alloy is 1.07 at%.

	$c_{Mn}^{\gamma\theta}$	$c_{Mn}^{\theta\gamma}$	$c_{Mn}^{\gamma\alpha}$	$c_{Mn}^{\alpha\gamma}$
823 K	0.37	1.13	10.3	1.06
958 K	0.773	1.81	3.89	0.942

3.3 Metallography for the Fe-Mn-C system

In Fig. 5, it is seen that the measured growth rate at low temperatures tends to be significantly slower than that calculated. It was not felt that there are any options in modifying the theory to obtain a better fit; for example, if the transfer of iron atoms across the interface is limiting, then we would not be able to explain the low-temperature data for Fe-C to such a high degree as illustrated in Fig. 3. Therefore, an Fe-0.8C-1.0Mn wt% alloy was made and the microstructure and growth rates of pearlite were measured for samples transformed at 958 K and 823 K, consistent to the experiments of Razik *et al.* About 500 g of steel sample was charged in a refractory crucible made of Al_2O_3 (OD 60 mm \times ID 52 mm \times H 100 mm).

The steel sample in the crucible was melted in a reaction chamber made of a quartz tube equipped with water cooled brass end caps in an induction furnace. Argon gas purified by passing through silica gel and Mg chips heated at

723 K (450 °C), was passed through the reaction chamber during the experiment and the sample solidified by natural cooling. The sample was sealed in an evacuated quartz tube, homogenised at 1250 °C for 48 h and hot-rolled at 1000 °C to 12 mm thickness and water quenched. The final chemical composition was Fe-0.79C-0.98Mn wt%. Specimens 3 mm diameter and 10 mm length were wire cut for dilatometer experiments (Dilatronic III, Theta Inc). The heat treatments were conducted in the dilatometer, with the sample austenitised 1100 °C and left for 10 min, cooled to transformation temperature, 823 K and 958 K and finally quenched to room temperature.

Transformation at 958 K led to the classical round pearlite colonies, the shape of which was affected only by the presence of the austenite grain boundaries Fig. 7. However, it is evident that the classical shape generated by the cooperative growth of ferrite and cementite clearly broke down during transformation at 823 K (Fig. 8). The transmission electron micrograph shown in Fig. 8d was obtained by machining a sample specifically from the spiky transformation product using focused ion-beam milling. It is evident that the cementite and ferrite do not share a common transformation front, with disconnected cementite particles present within the predominantly ferritic matrix. When this happens, the growth rate should decrease because the lack of cooperation would increase the diffusion distances, and with the shapes observed, boundary diffusion at the transformation front would make a smaller contribution since the flux becomes less parallel to the interface.

It could be argued that the spiky transformation product observed for 823 K is in fact bainite. Experiments were therefore done to see whether this non-cooperative growth product results in the surface relief that is typical of bainite, as opposed to diffusional transformation produces that only result in volume changes. Metallographically polished but un-etched samples were heat treated using the dilatometer, and then inspected for surface relief. The sample was austenitised at 1100 °C and left for 10 min, cooled to transformation temperature, 823 K, stayed for 3.6 s, then quenched to room temperature. Hardness indents were used as fiducial marks to correlate surface relief with the same area after very light etching using 2% nital in ethanol with less than 10 s. Fig. 9 shows with clarity that the only surface relief is from the few plates of bainite that formed during the quench, with neither the spiky nor regular bainite exhibiting any such upheavals.

Table 2 compares our experimental data, derived specifically from isolated, spherical pearlite colonies, using the largest colony method, against those from ref. [31]. There is good agreement for transformation at 958 K but our growth rate for 823 K is larger and more consistent with the calculated values. We are not able to explain this discrepancy at this moment. It is noteworthy that neutron depolarisation experiments [36] gave a pearlite growth rate of $1.19 \times 10^{-7} \text{ m s}^{-1}$ at 953 K in a Fe-0.715C-0.611Mn-0.266Cr-0.347Si wt%, consistent

with the present work if the differences in substitutional solute concentrations are neglected.

Table 2

Comparison of measured growth rate [31] against our experimental data.

	958 K	823 K
Measured rate / m s^{-1} [31]	1.63×10^{-7}	9.54×10^{-6}
Measured rate / m s^{-1} , current work	1.09×10^{-7}	2.30×10^{-5}
Calculated rate / m s^{-1}	1.87×10^{-7}	3.12×10^{-5}

4 Conclusions

It has been possible to find solutions that satisfy local equilibrium at the pearlite transformation front for both the Fe-C and Fe-C-Mn systems. The method used to achieve this involves independent calculations of growth velocity based on each solute, followed by iteration to achieve the same growth rate irrespective of solute. The method takes into account both boundary and volume diffusion, gives satisfactory closure between theory and experiment.

The largest discrepancy between published data on the Fe-Mn-C system and theory exists at the lowest transformation temperature, where we have demonstrated that two forms of pearlite form, one represented by the regular spheroidal colony and the other by a spiky morphology where the cooperation between ferrite and cementite breaks down. In such circumstances, the growth rate equations derived for cementite and ferrite sharing a common transformation front with austenite do not apply. When the growth rate is measured only for the spheroidal colonies of pearlite, even the low temperature data closely approximate theory.

Finally, it has been demonstrated that the spiky transformation product does not lead to the surface relief effect associated with displacive transformations.

Acknowledgments: Seung-Woo Seo especially thanks Minsu Kim and Hyun Woo Mun for their help with the experiments.

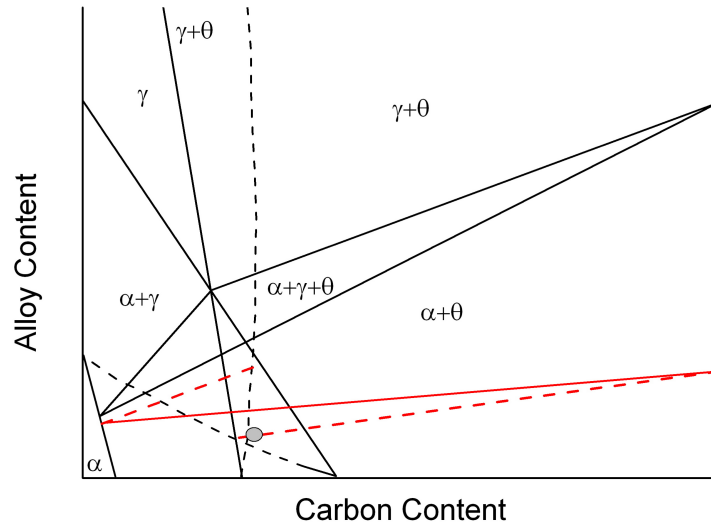


Fig. 1. Fe-Mn-C phase diagram and tie-lines (red) used in [11].

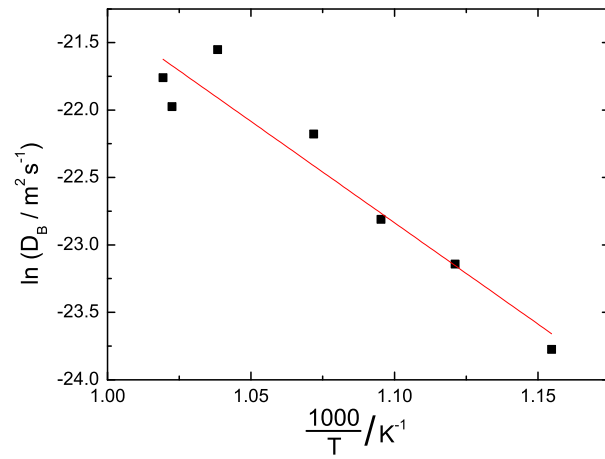


Fig. 2. Arrhenius plot from which D_B was derived based on experimental data on Fe-0.8 wt% C steel assuming mixed diffusion-controlled pearlite growth.

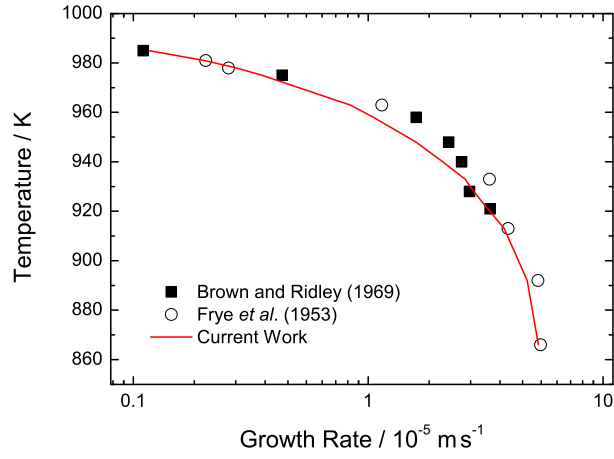


Fig. 3. Calculated growth rate of pearlite for mixed diffusion model compared against experimental data.

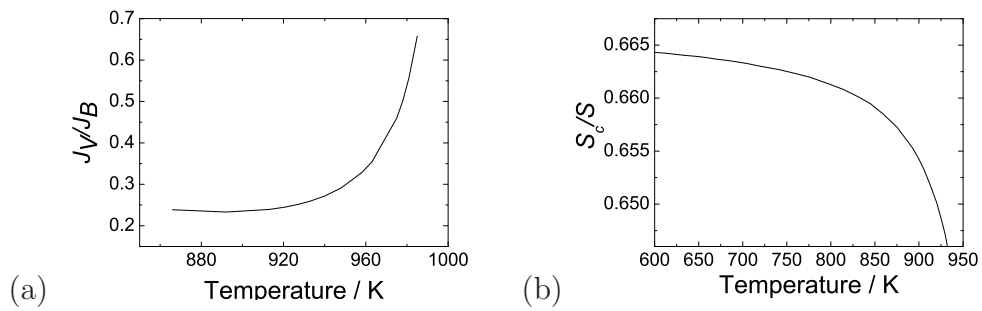


Fig. 4. (a) The ratio of volume to boundary flux versus temperature in Fe-C eutectoid steel. (b) The ratio of critical interlamellar spacing, S_C to S as a function of temperature.

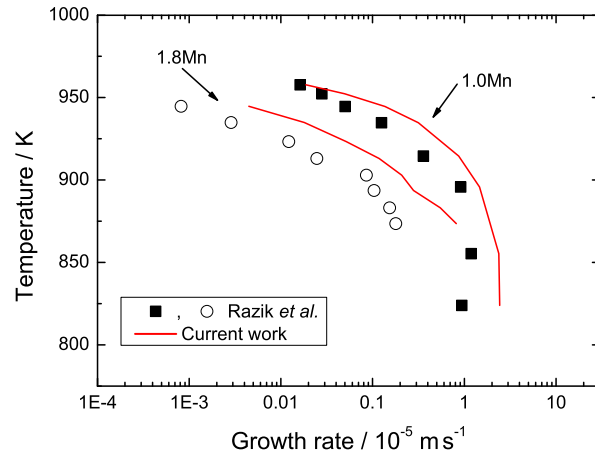


Fig. 5. Mixed diffusion-controlled model applied to 1.0 and 1.8 wt%Mn eutectoid steels and experimental data for comparison.

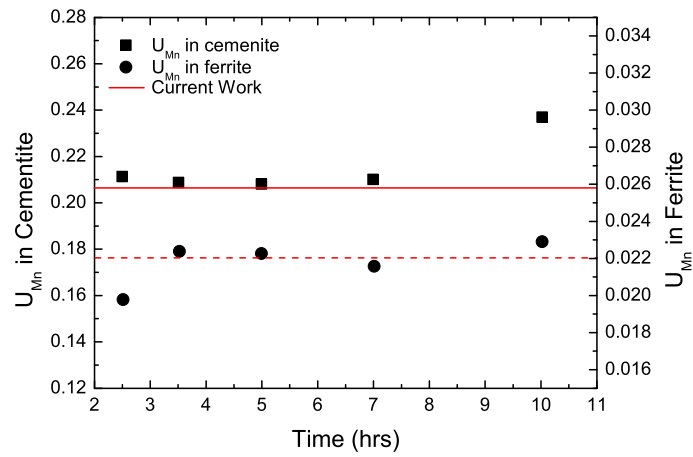


Fig. 6. Mixed diffusion-controlled model predicts the interface composition of pearlite in Fe-3.50 at%Mn-2.46 at%C steel at 898 K. U_{Mn} is the ratio of the Mn to Fe atoms.

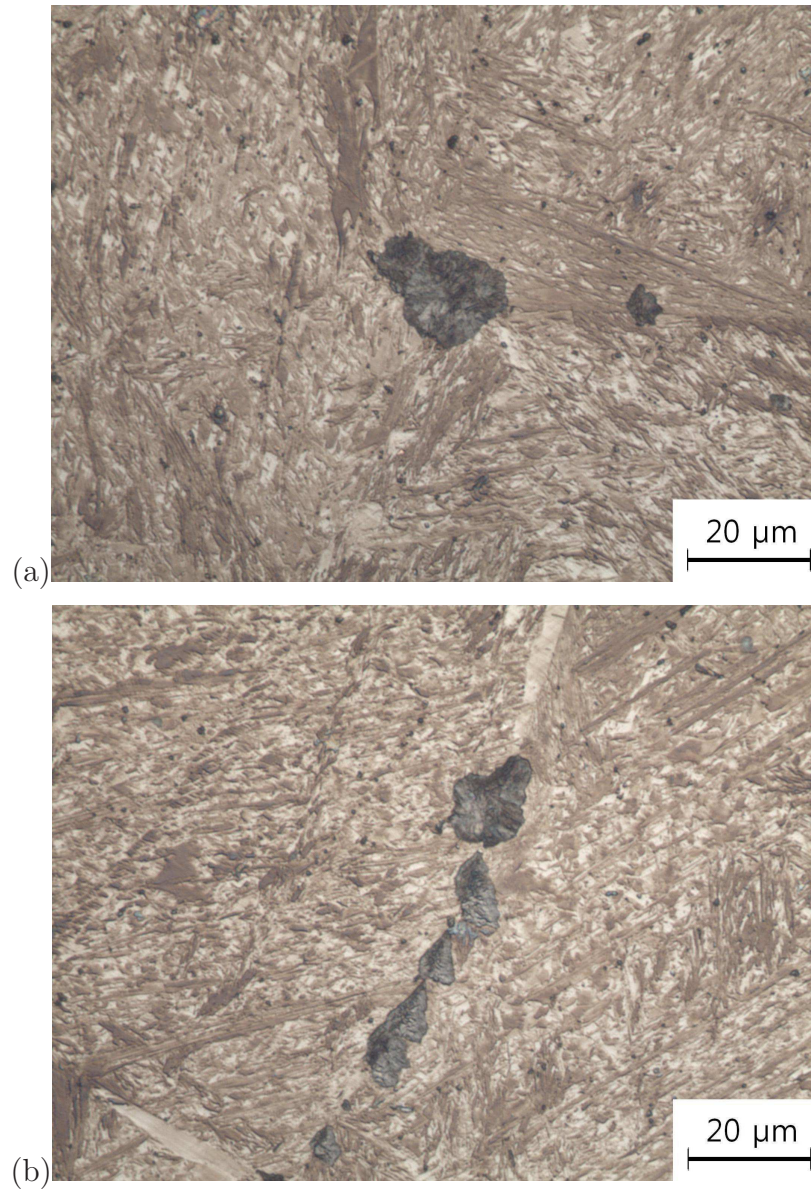


Fig. 7. Microstructure of isothermal transformation at 957 K held for 2 min by optical micrograph. (a) and (b) show spherical shape of typical pearlite morphology.

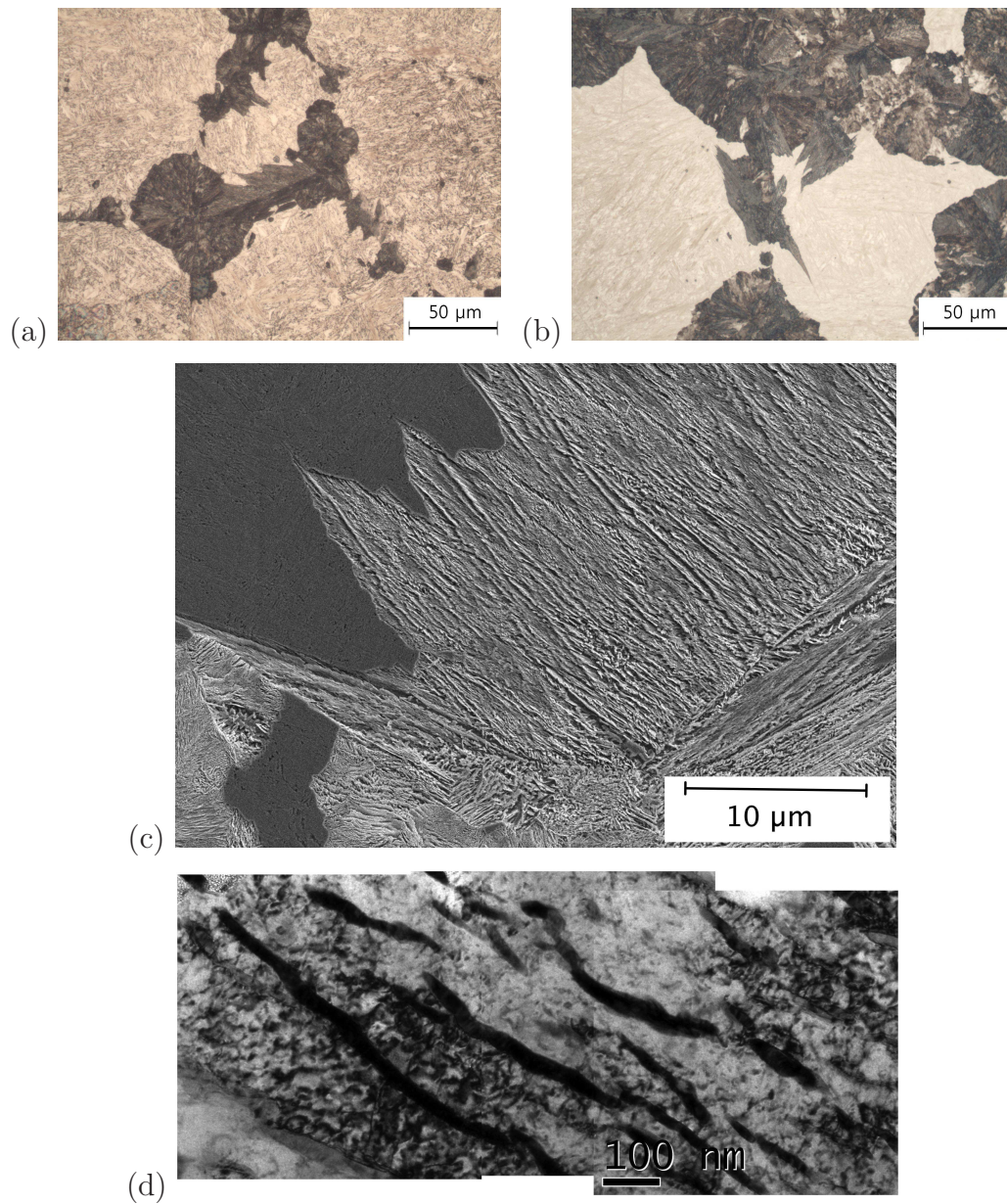


Fig. 8. Optical micrographs of isothermal transformation at 823 K held for (a) 3.6 s and (b) 5 s. (c) Scanning electron micrograph (3.6 s). (d) Transmission electron micrograph (3.6 s).

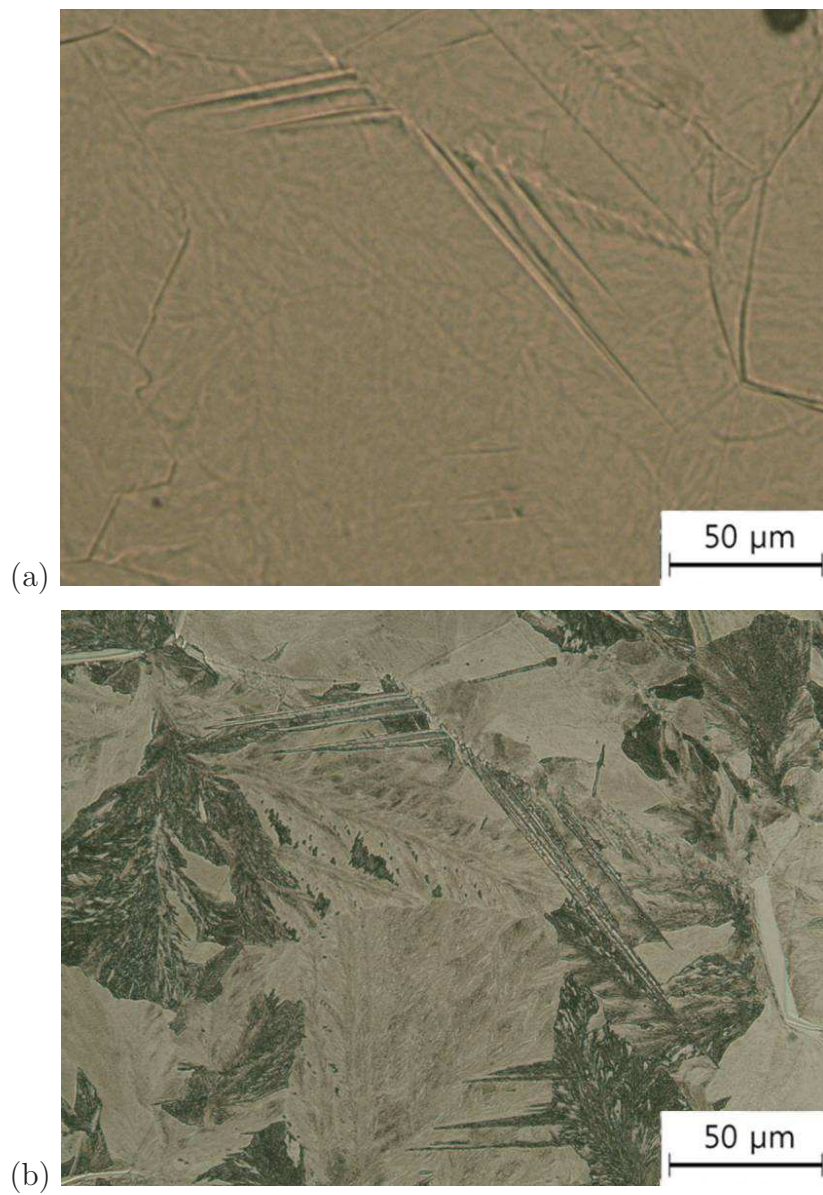


Fig. 9. Corresponding images from the surface relief experiments. The dark-etching spiky form of pearlite where the ferrite and cementite do not grow at a common transformation front does not exhibit any surface upheavals. Nor does any of the pearlite. It is only the few plates of lighter-etching bainite that show the surface relief. (a) Unetched sample, (b) after light etching. Samples transformed at 823 K for 3 s.

References

1. M. Hillert: 'The formation of pearlite', In: V. F. Zackay, and H. I. Aaronson, eds. *Decomposition of austenite by diffusional processes*. New York, USA: Interscience, 1962:197–237.
2. C. Zener: 'Kinetics of the decomposition of austenite', *Trans. Am. Inst. Min. Metall. Engng.*, 1946, **167**, 550–595.
3. M. Hillert: 'Role of interfacial energy during solid–state phase transformations', *Jernkontorets Annaler*, 1957, **141**, 757–789.
4. M. Hillert: 'The role of interfaces in phase transformations', In: *Mechanism of Phase Transformations in Crystalline Solids*. Monograph and Report Series No. 33, London, U.K.: Institute of Metals, 1970:231–247.
5. N. Ridley: 'The pearlite reaction', In: A. R. Marder, and J. I. Goldstein, eds. *Phase Transformations in Ferrous Alloys*. Warrendale, Pennsylvania, USA: TMS–AIME, 1984:201–236.
6. J. W. Christian: *Theory of Transformations in Metals and Alloys*, Part II: 3 ed., Oxford, U. K.: Pergamon Press, 2003.
7. B. E. Sundquist: 'The edgewise growth of pearlite', *Acta Metallurgica*, 1968, **16**, 1413–1427.
8. M. Hillert: 'On theories of growth during discontinuous precipitation', *Metallurgical Transactions*, 1972, **3**, 2729–2741.
9. K. Hashiguchi, and J. S. Kirkaldy: 'Pearlite growth by combined volume and phase boundary diffusion', *Scandinavian Journal of Metallurgy*, 1984, **13**, 240–248.
10. A. S. Pandit, and H. K. D. H. Bhadeshia: 'Mixed diffusion-controlled growth of pearlite in binary steel', *Proceedings of the Royal Society A*, 2011, **467**, 508–521.
11. A. S. Pandit, and H. K. D. H. Bhadeshia: 'The growth of pearlite in ternary steels', *Proceedings of the Royal Society A*, 2011, **467**, 2948–2961.
12. K. Nakajima, M. Apel, and I. Steinbach: 'The role of carbon diffusion in ferrite on the kinetics of cooperative growth of pearlite: A multi-phase field study', *Acta Materialia*, 2006, **54**, 3665–3672.
13. I. Steinbach, and M. Plapp: 'Pearlite revisited', *Continuum Mechanics and Thermodynamics*, 2012, **24**, 665–673.
14. H. K. D. H. Bhadeshia: 'Diffusional formation of ferrite in iron and its alloys', *Progress in Materials Science*, 1985, **29**, 321–386.
15. M. Hillert: 'Paraequilibrium': Tech. Rep., Swedish Institute for Metals Research, Stockholm, Sweden, 1953.
16. J. S. Kirkaldy, and R. C. Sharma: 'Stability principles for lamellar eutectoid(ic) reactions', *Acta Metallurgica*, 1980, **28**, 1009–1021.
17. G. R. Purdy, D. H. Weichert, and J. S. Kirkaldy: 'The growth of proeutectoid ferrite in ternary Fe–C–Mn austenites', *Trans. TMS-AIME*, 1964, **230**, 1025–1034.
18. D. E. Coates: 'Diffusional growth limitation and hardenability', *Metallurgical Transactions*, 1973, **4**, 2313–2325.

19. S. A. Al-Salman, G. W. Lorimer, and N. Ridley: ‘Pearlite growth kinetics and partitioning in a Cr-Mn eutectoid steel’, *Metallurgical Transactions A*, 1979, **10A**, 1703–1709.
20. J. Chance, and N. Ridley: ‘Chromium partitioning during isothermal transformation of a eutectoid steel’, *Metallurgical Transactions A*, 1981, **12A**, 1205–1213.
21. C. R. Hutchinson, R. E. Hackenberg, and G. J. Shiflet: ‘The growth of partitioned pearlite in Fe-C-Mn steels’, *Acta Materialia*, 2004, **52**, 3565–3585.
22. S. Lenka, S. Kundu, S. Chandra, and S. B. Singh: ‘Effect of recalescence on microstructure and phase transformation in high carbon steel’, *Materials Science and Technology*, 2013, **29**, 715–725.
23. D. Luo, M. J. Peet, S. W. Ooi, P. Yan, Z. Yin, and H. K. D. H. Bhadeshia: ‘Spheroidisation of hypereutectoid state of nanostructured bainitic steel’, *Materials Science and Technology*, 2014, **30**, 1282–1286.
24. R. S. Qin, A. Rahnama, W. J. Lu, and B. E.-B. X. F. Zhang and: ‘Electropulsed steels’, *Materials Science and Technology*, 2014, **30**, DOI 10.1179/1743284714Y.00000000533.
25. M. M. Aranda, B. Kim, R. Rementeria, C. Capdevila, and C. G. de Andrés: ‘Effect of prior austenite grain size on pearlite transformation in a hypoeutectoid Fe-C-Mn steel.’, *Metallurgical & Materials Transactions A*, 2014, **45**, 1778–1786.
26. R. T. van Tol, L. Zhao, and J. Sietsma: ‘Kinetics of austenite decomposition in manganese-based steel’, *Acta Materialia*, 2014, **64**, 33–40.
27. J. Li, and L. Wei: ‘Effects of high magnetic field on isothermal pearlite transformation and microstructure in a hypereutectoid steel’, *Journal of Magnetism and Magnetic Materials*, 2014, **362**, 159–164.
28. J. O. Andersson, T. Helander, L. Hoglund, P. Shi, and B. Sundman: ‘Thermo-Calc & DICTRA, computational tools for materials science’, *CALPHAD*, 2002, **26**, 273–312.
29. J. H. Frye Jr, E. E. Stansbury, and D. L. McElroy: ‘Absolute Rate Theory Applied to Rate of Growth of Pearlite’, *Trans. AIME*, 1953, **197**, 219–224.
30. D. Brown, and N. Ridley: ‘Kinetics of the pearlite reaction in high-purity nickel eutectoid steels’, *Journal of the Iron and Steel Institute*, 1969, **207**, 1232–1240.
31. N. A. Razik, G. W. Lorimer, and N. Ridley: ‘An investigation of manganese partitioning during the austenite-pearlite transformation using analytical electron microscopy’, *Acta Metallurgica*, 1974, **22**, 1249–1258.
32. R. Trivedi, and G. M. Pound: ‘Effect of concentration dependent diffusion coefficient on the migration of interphase boundaries’, *Journal of Applied Physics*, 1967, **38**, 3569–3576.
33. R. F. Mehl, and W. C. Hagel: ‘The austenite:pearlite reaction’, *Progress in Metal Physics*, 1956, **6**, 74–134.
34. J. W. Cahn, and W. C. Hagel: ‘Theory of pearlite reaction’, In: V. F. Zackay, and H. I. Aaronson, eds. *Decomposition of Austenite by Diffusional*

- Processes*. New York: Intersciences, 1962:131–192.
35. S. E. Offerman, L. J. G. W. van Wilderen, N. H. van Dijk, J. Sietsma, M. th.Rekvelde, and S. van der Zwaag: ‘In situ study of pearlite nucleation and growth during isothermal austenite decomposition in nearly eutectoid steel’, *Acta Materialia*, 2003, **51**, 3927–3938.
 36. S. E. Offerman, N. H. van Dijk, J. Sietsma, S. Grigull, E. M. Lauridsen, L. Margulies, H. F. Poulsen, M. T. Rekvelde, and S. van der Zwaag: ‘Grain nucleation and growth during phase transformations’, *Science*, 2002, **298**, 1003–1005.
 37. J. Fridberg, L.-E. Torndahl, and M. Hillert: ‘Diffusion in iron’, *Jernkontorets Annaler*, 1969, **153**, 263–276.